Proceedings of the 12th International Symposium UFPS, Vilnius, Lithuania 2004

Carrier Dynamics in Quantum Cascade Lasers

P. Harrison[a], D. Indjin[a], V.D. Jovanović[a], A. Mirčetić[b], Z. Ikonić[a], R.W. Kelsall[a], J. McTavish[a], I. Savić[a], N. Vukmirović[a,b] and V. Milanović[b,a]

[a]School of Electronic and Electrical Engineering, University of Leeds
Leeds LS2 9JT, United Kingdom
[b]Faculty of Electrical Engineering, University of Belgrade
Bulevar kralja Aleksandra 73, 11120 Belgrade, Serbia and Montenegro

A fully quantum-mechanical model for carrier scattering transport in semiconductor intersubband devices was applied to modelling of carrier dynamics in quantum cascade lasers. The standard model uses the envelope function and effective mass approximations to solve electron band structure under an applied bias. The $\boldsymbol{k}\cdot\boldsymbol{p}$ model has been employed in p-type systems where the more complex band structure requires it. The resulting wave functions are then used to evaluate all relevant carrier–phonon, carrier–carrier and alloy scattering rates from each quantised state to all others within the same and the neighbouring period. This piece of information is then used to construct a rate equation for the equilibrium carrier density in each subband and this set of coupled rate equations are solved self-consistently to obtain the carrier density in each eigenstate. The latter is a fundamental description of the device and can be used to calculate the current density and gain as a function of the applied bias and temperature, which in turn yields the threshold current and expected temperature dependence of the device characteristics. A recent extension which includes a further iteration of an energy balance equation also yields the electron (or hole) temperature over the subbands. This paper will review the method and describe its application to mid-infrared and terahertz, GaAs, GaN, and SiGe cascade laser designs.

PACS numbers: 42.60.–v

1. Introduction

The quantum cascade laser (QCL) has demonstrated an impressive extension of the infrared frequency range and until recently could be operated at wavelengths as long as 160 μm. Recent experience in the design of novel QCLs clearly shows that systematic and compact theoretical modelling is a necessary step towards

effective practical implementation, improvements of the existing structures, and the understanding of physical processes [1, 2]. The laser gain depends on the scattering rates between different subbands and also between different in-plane momentum states within a subband (carrier heating / cooling effects). These effects have been extensively studied in QCLs based on conduction band intersubband transitions. One approach relies on self-consistent solutions of rate equations [1−3]. Another approach uses the microscopic, and computationally more demanding Monte Carlo technique [4]. Although the latter does not make the assumption of equilibrium-like carrier distributions over states within any single subband, and therefore gives a deeper insight into the electron dynamics, the former are much faster while still giving quite good estimates of device characteristics. In p-type system the problem is generally similar to the case of n-type cascades, but is more complex because the hole subband structure and scattering rates are anisotropic and strongly dependent on the in-plane momentum of the hole states. In this paper we will present a brief overview of the model limited only to the applications on n-type QCLs while results for both p- and n-type structure will be presented (for more information about p-type QCL modelling see Ref. [5]).

2. The model

Consider a QCL structure with a large number of periods (each containing of multiple quantum well) in an externally applied electric field. The energy spectrum is formally continuous, but to a very good approximation can be considered as consisting of quasi-discrete states (resonances). Based on the wave function localization properties, these states can be associated to different periods of the QCL, so that each period has an identical set of N states in the energy range of interest. Electron scattering occurs between states within the same period, and between states associated to different periods, the latter clearly becoming less effective for more distant periods because of reduced wave function overlap. Assuming an identical electron distribution in each period, one may consider some "central" period and take its P nearest neighbours on either side, and write the scattering rate equations in the steady-state:

$$\sum_{j=1,j\neq i}^{N} n_j W_{j,i} - n_i \sum_{j=1,j\neq i}^{N} W_{i,j} + \sum_{k=1}^{P} \sum_{j=1,j\neq i}^{N} \big[n_j (W_{j,i+kN} + W_{j+kN,i}) - n_i (W_{i+kN,j} + W_{i,j+kN}) \big] = 0, \tag{1}$$

where $i + kN$ is the i-th state of the k-th neighbouring period, $W_{i,j}$ is the total scattering rate from state i into state j, n_i is the electron concentration of the i-th state. The first two sums in Eq. (1) are due to intra-period, and the third — due to inter-period scattering. After solving for electron densities n_i, macroscopic parameters of the system like current density, threshold current, and laser gain can be estimated. The scattering time $W_{\mathrm{i,f}}$ is a function of both n_{i} and n_{f}, the

initial and final subband populations, hence, this set of equations has to be solved self-consistently using an iterative procedure. At equilibrium, the rate at which the electron distributions gain kinetic energy (relative to the particular subband minimum) through scattering, will balance with the rate at which they lose kinetic energy to the lattice. Despite the fact that electron–electron scattering is elastic as far as total energy is concerned, intersubband electron–electron transitions do convert potential energy into kinetic energy (or vice versa). From the viewpoint of this work this would lead to an increase (decrease) in the total kinetic energy of a subband population, because the potential energy as defined here includes the quantised component of the kinetic energy. Hence, the kinetic energy balance condition in case where only electron-LO phonon and electron–electron processes are included, can be written as [2]:

$$\Delta = \sum_{\text{em.,abs.,e}-\text{e}} \sum_{\text{f}} \sum_{\text{i}} n_{\text{i}} W_{\text{i,f}} (E_{\text{i}} - E_{\text{f}} + \delta E) = \Delta_{\text{e}-\text{LO}} + \Delta_{\text{e}-\text{e}} = 0, \tag{2}$$

where $E_{\text{i}} - E_{\text{f}}$ is the subband separation, and the change in energy δE is equal to $-E_{\text{LO}}$ for phonon emission (em.), $+E_{\text{LO}}$ for phonon absorption (abs.), and zero for electron–electron (e–e) scattering. Hence, $\Delta_{\text{e}-\text{LO}}$ is net electron-LO phonon, and $\Delta_{\text{e}-\text{e}}$ is net electron–electron contribution in the balance equation. The method is easily extendable in case that other scattering mechanisms (electron-acoustical phonon, impurity and alloy scattering, etc.) should be taken into account. The next step of the procedure, is to vary the electron temperature (assumed to be the same for all subbands) until the kinetic energy balance equation Eq. (2) is satisfied self-consistently.

The current density can be calculated by subtracting the current density component due to electrons scattering into the next periods of the QCL from the component due to electrons scattering back. If we put a reference plane somewhere in the injection barrier of the central period, the current density flowing through that cross-section can be written as:

$$J = \sum_{k=1}^{P} \sum_{i=1}^{N} \sum_{j=1}^{N} k \cdot n_i (W_{i,j+kN} - W_{i+kN,j}). \tag{3}$$

The factor k in the summation, effective for non-nearest-neighbour scattering, comes from scatterings from any QCL period left of the centre period into any period right of it, or vice versa (i.e. skipping the central period, but going through the reference plane). In order to reduce the number of scattering rate processes necessary to calculate the electron distribution and the corresponding current density (note that the number of total scattering rate processes is equal to $N^2(2P+1)-N$), we introduce the "tight-binding" approximation assuming that only a few closest neighbours interact, and set $P = 2$. The choice of quantum scattering mechanisms depends on the material and doping density, as well as wavelength. For example in the novel GaAs-based THz QCLs the energy separation between most of subbands

is smaller than the LO phonon energy and electron–electron scattering becomes the dominant scattering mechanism, hence necessitating a large number of possibly relevant scattering processes to be accounted for [3]. To extract the output characteristics of QCLs, one has to change the electric field F (i.e. the applied voltage) and calculate the modal gain G_{M} and the total current density J for each value of the field.

3. Applications

Electric field vs. current density characteristics at lattice temperature $T_{\mathrm{latt}} = 20$ K is shown in Fig. 1a for original GaAs/AlGaAs terahertz QCL [6]. Under the assumption $T_{\mathrm{e}} = T_{\mathrm{latt}}$ (dashed line), the $F - J$ curves show current density saturation and negative differential resistance (NDR) features at very low currents, which are not consistent with experimental results [6]. We find with the full calculation (solid line), which includes the energy balance, that current is predicted to saturate at ~ 680 A/cm^2 in reasonable agreement with that measured at ~ 820 A/cm^2. Calculated values of the average electron temperature are also shown. A schematic diagram of analysed structure is given in the inset. The calculations also show (see Fig. 1b) that, up to the NDR feature, T_{e} can be approximated as linear function $T_{\mathrm{e}} \approx T_{\mathrm{latt}} + \beta J$, where $\beta \sim 52$ K/(kA cm^{-2}). The most recent micro-probe photoluminscence measurement but in a different terahertz QCLs design [7] also suggests linear $T_{\mathrm{e}}(J)$ dependence with $\beta \sim 69{-}77$ K/(kA cm^{-2}), in close agreement with our findings.

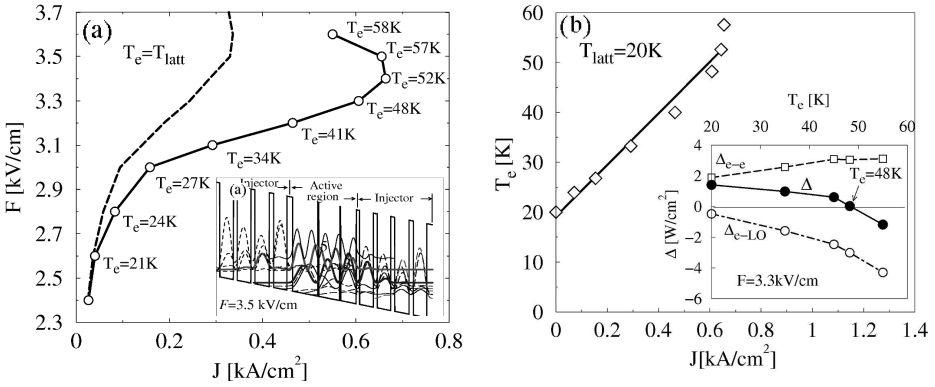

Fig. 1. (a) Electric field vs. current density characteristics in GaAs/AlGaAs THz QCL at lattice temperature $T_{\mathrm{latt}} = 20$ K. A schematic diagram of analysed structure is given in the inset. (b) Calculated electron temperature vs. current density in the terahertz QCL at lattice temperature $T_{\mathrm{latt}} = 20$ K. The symbols are the calculated results and the line represents the least square fit used to derive the values of coupling constant β. An example of electron temperature evaluation for specific value of electric field ($F = 3.3$ kV/cm) is shown in the inset (see Eq. (2)).

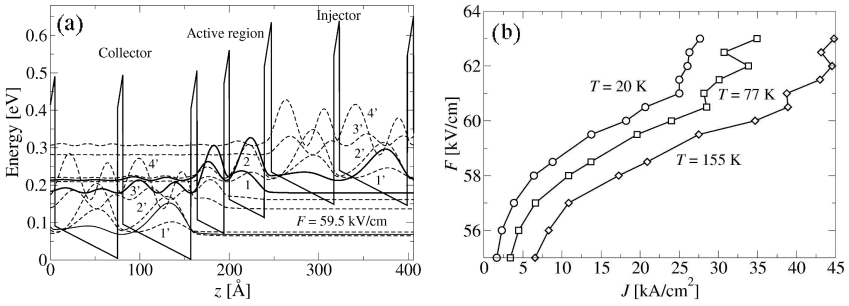

Fig. 2. (a) A schematic diagram of quasi-bound energy levels and associated wave functions squared for an injector-active region-collector segment of GaN/AlGaN THz QCL. The layer sequence of one period of structures, in nanometers, from right to left from the injection barrier: **0.7**, 3, **0.6**, 3.9, **0.8**, 7, **0.6**, 7.6. The normal script denotes the wells and bold — the barriers. (b) Electric field-current characteristics calculated for three temperatures.

The designs for GaN/AlGaN quantum cascade lasers emitting 38 μm ($\Delta E \sim$ 34 meV — GaAs forbidden Restrahlenband) are shown in Fig. 2a [8]. The quasi-bound energies and associated wave functions are calculated with the intrinsic electric field induced by piezoelectric and spontaneous polarization included. The population inversion up to 25% is found resulting in feasible laser action [8]. Figure 2b shows electric field-current characteristics for three different lattice temperatures. The characteristics exhibit current density saturation as well as the region of negative differential resistance. Saturation occurs for the electric field value high enough to misalign the upper laser level and ground injector states, i.e. positioning the upper laser level in energy below the ground injector states. Figure 3 shows the population inversion $\Delta n = n_3 - n_1$, and populations of the active laser levels as a function of lattice temperature in GaN/AlGaN QCL. The inversion slightly decreases at higher temperatures due to increased depopulation rate from the upper into the lower laser level. The GaN/AlGaN design features

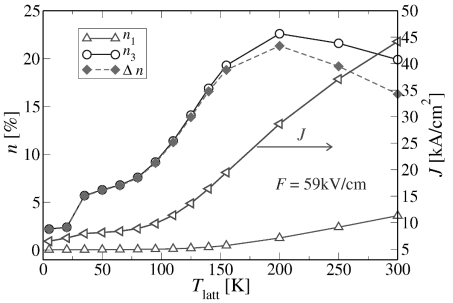

Fig. 3. The population inversion $\Delta n = n_3 - n_1$, the subband populations of the upper (n_3) and the lower (n_1) laser levels (left axis) and current density (right axis) as a function of lattice temperature.

good thermal stability predominantly due to larger LO-phonon energy compared to lasing energy. A significant increase in current density above $T_{\rm latt} = 100$ K is also predicted in this structure.

Self-consistent energy balance simulations, within either the single- or multiple-temperature model (in the latter case each subband having its own carriers temperature) have been performed for p-Si/SiGe quantum cascade structures [9]. In this system there are no polar optical phonons, and the calculation includes nonpolar acoustic and optical phonon (deformation potential) scattering, alloy disorder scattering, and hole–hole scattering. Results for a simple strain--balanced cascade, comprising the stack of alternating wells and barriers — 16 monolayer (4.41 nm) $Ge_{0.3}Si_{0.7}$ wells and 8 monolayer (2.15 nm) wide Si barriers — grown on a $Ge_{0.2}Si_{0.8}$ virtual substrate, are shown in Figs. 4 and 5. The

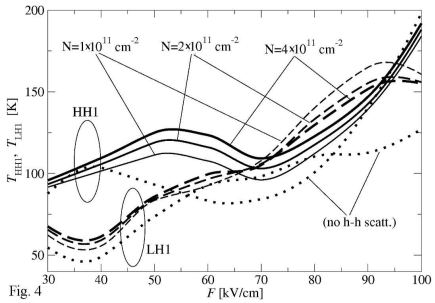

Fig. 4

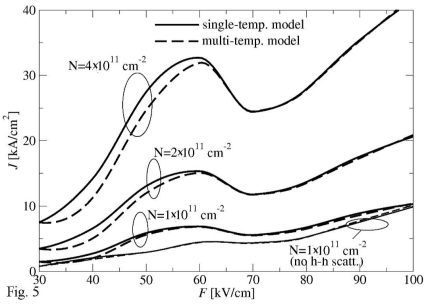

Fig. 5

Fig. 4. The bias dependence of the HH1 and LH1 subband temperatures in the p-SiGe cascade described in the text, calculated within the multiple-temperature model, for different values of hole sheet density per period, at $T_{\rm latt} = 20$ K.

Fig. 5. The bias dependence of the current density in the p-SiGe cascade described in the text, calculated within the multiple-temperature model, for different values of hole sheet density per period, at $T_{\rm latt} = 20$ K.

cascade has just two low-lying states per period, the ground HH1 and the first — excited, LH1 state; the next, HH2 state is sufficiently higher in energy to remain almost inaccessible to holes throughout the range of biases used in the calculation. The LH1–HH1 energy spacing in the Si/SiGe system is primarily determined by the strain in the quantum well layers, and here amounts to 27.5 meV. In a biased cascade the alignment of the HH1 state from the preceding (higher) well and the LH1 state of the next (lower) well at $\boldsymbol{k}_{\|} = 0$ occurs at a field of 42 kV/cm. However, for finite $\boldsymbol{k}_{\|}$ the alignment appears at different fields, because of the different dispersions of the HH and LH states, so the phenomenon of resonance is not so strong as in the case of n-type heterostructures. As the bias field varies, the spacing between LH1 and HH1 states of the same well changes only slightly, and most of the potential drop per period manifests in the displacement of the sets of states belonging to adjacent periods.

The hole temperatures, calculated for different values of the total hole sheet density in this cascade, Fig. 4, depend nonmonotonically on the bias field, and may be quite different in the two subbands for some values of bias, or similar for other values. Also, they increase with increasing hole density, but this dependence is relatively weak. In a conduction subband cascade the different values of carrier temperatures would hardly have any effect on the optical spectra, because of the identical dispersions of subbands and the wavevector conservation in optical transitions, but may be important in transport. On the other hand, in p-type cascades the different values of hole temperatures are important for intersubband optical properties as well, because these depend on the hole distributions in the strongly and *unequally* dispersive subbands.

Interestingly, the calculated current density is not much affected by the type of calculation (single- or multiple-temperature model), as shown in Fig. 5, and the same applies to the population of the two states. Throughout the range of parameters explored in these calculations, the LH1 population remains smaller than that of the HH1 state, implying the existence of population inversion on the interwell HH1→LH1 optical transition. There is a region (60–70 kV/cm) of NDR, and this is more prominent for larger hole densities, because of the increasing role of hole–hole scattering. NDR appears as the interplay of the bias-dependent rate of the interwell processes of this type (which favour small spacing between subbands), and the bias-dependent asymmetry of right → left and left → right transfers, which requires somewhat larger subband spacings. Although the peak/valley current ratio may not be very large, there exists the possibility of domain formation in the cascade when biased in the above range.

4. Conclusion

In summary we reviewed the method for physical modelling and describe its application to design and optimisation of GaAs, GaN, SiGe-based cascade lasers.

References

[1] D. Indjin, P. Harrison, R.W. Kelsall, Z. Ikonić, *Appl. Phys. Lett.* **81**, 400 (2002).

[2] P. Harrison, D. Indjin, R.W. Kelsall, *J. Appl. Phys.* **92**, 6921 (2002).

[3] D. Indjin, P. Harrison, R.W. Kelsall, Z. Ikonić, *Appl. Phys. Lett.* **82**, 1347 (2003).

[4] R.C. Iotti, F. Rossi, *Phys. Rev. Lett.* **87**, 146603 (2001).

[5] Z. Ikonić, P. Harrison, R.W. Kelsall, *J. Appl. Phys.* **96**, 6803 (2004).

[6] R. Köhler, A. Tredicucci, F. Beltram, H.E. Beere, R. Iotti, F. Rossi, *Nature* **417**, 156 (2002).

[7] M.S. Vitiello, V. Sapgnolo, G. Scamarcio, B.S. Williams, S. Kumar, Q. Hu, J.L. Reno, presented at *Proc. 6th Int. Conf. in Mid-infrared Optoelectronics and Materials and Devices, St. Petersburg (Russia), June 2004.*

[8] V.D. Jovanović, D. Indjin, Z. Ikonić, P. Harrison, *Appl. Phys. Lett.* **84**, 2995 (2004).

[9] Z. Ikonić, R.W. Kelsall, P. Harrison, *Phys. Rev. B* **69**, 235308 (2004).